

# Underactuated Robotic Gripper With Fiber-Optic Force Sensing Tendons

Jaehyun Yi , Graduate Student Member, IEEE, Byungchul Kim , Kyu-Jin Cho , Member, IEEE,  
and Yong-Lae Park , Member, IEEE

**Abstract**—We present a novel design for a multi-fingered robotic gripper, featuring underactuation and fiber-optically sensorized tendons for force sensing, inspired by the Golgi tendon organs found in biological muscles. Our robotic gripper comprises three rigid fingers, each with three joints: the metacarpophalangeal (MCP), proximal interphalangeal (PIP), and distal interphalangeal (DIP). To enable flexion and extension, each is actuated using a combination of two types of tendons: an active tendon and three passive tendons. The active tendon is a single-mode optical fiber with an embedded fiber Bragg grating (FBG) that detects the tension of the fiber during the gripper’s grasping motions. Meanwhile, three elastic passive tendons, made of soft elastomer and located on the dorsal side of the finger, retract the finger to its initial extended position upon the release of the active tendon. Through the measurement of the wavelength shift of the FBG, induced by the strain applied to the fiber-optic tendon, we can convert this data into force values, facilitating grasping force control. Our proposed gripper is tested with objects of varying stiffness and demonstrates the force-sensing capability of the sensorized tendons.

**Index Terms**—Underactuated robots, grippers and other end-effectors, tendon/wire mechanism, force and tactile sensing, force control.

Manuscript received 2 May 2023; accepted 8 September 2023. Date of publication 13 September 2023; date of current version 10 October 2023. This letter was recommended for publication by Associate Editor M. Gauthier and Editor A. Banerjee upon evaluation of the reviewers’ comments. This work was supported in part by the National Research Foundation (NRF) under Grants RS-2023-00208052 and 2021R1A2C2093790, and in part by the Institute of Information & Communications Technology Planning & Evaluation (IITP) under Grant 2021-0-00896, both funded by the Korean Government (MSIT). (Corresponding author: Yong-Lae Park.)

Jaehyun Yi, Kyu-Jin Cho, and Yong-Lae Park are with the Department of Mechanical Engineering, Seoul National University, Seoul 08826, Republic of Korea, also with the Institute of Advanced Machines and Design, Seoul National University, Seoul 08826, Republic of Korea, also with the Institute of Engineering Research, Seoul National University, Seoul 08826, Republic of Korea, and also with the Soft Robotics Research Center, Seoul National University, Seoul 08826, Republic of Korea (e-mail: ljtheman@snu.ac.kr; kjcho@snu.ac.kr; ylpark@snu.ac.kr).

Byungchul Kim is with the Department of Mechanical Engineering, Seoul National University, Seoul 08826, Republic of Korea, also with the Institute of Advanced Machines and Design, Seoul National University, Seoul 08826, Republic of Korea, also with the Institute of Engineering Research, Seoul National University, Seoul 08826, Republic of Korea, also with the Soft Robotics Research Center, Seoul National University, Seoul 08826, Republic of Korea, and also with the Computer Science and Artificial Intelligence Laboratory, Massachusetts Institute of Technology, Cambridge, MA 02139 USA (e-mail: bckim@mit.edu).

This letter has supplementary downloadable material available at <https://doi.org/10.1109/LRA.2023.3315204>, provided by the authors.

Digital Object Identifier 10.1109/LRA.2023.3315204

## I. INTRODUCTION

As robots increasingly permeate our daily lives, dexterous manipulation of various objects has become one of the most important functions that robots are expected to equip with, leading to research and development of novel designs and mechanisms for robotic grippers [1], [2]. However, conventional force-sensing mechanisms, such as load cells [3], [4] or tactile sensors [5], [6], which are not necessarily physically combined with the actuators, do not provide direct information on the states of the actuators. The presence of proprioceptors in biological muscles, such as the Golgi tendon organ (GTO) and the muscle spindle, however, makes a significant distinction between conventional robotic grippers and the human hands. The GTO senses changes in muscle tension, whereas the muscle spindle detects changes in muscle length and speed [7], [8]. This information is essential for identifying the characteristics of the objects to be handled with dexterity and stability, including texture, size, shape, and stiffness. Thus, integrating proprioceptive sensing into actuators offers novel solutions to overcome the limitations of grasping and manipulation strategies in conventional robots [9], [10], [11], [12], [13], [14].

In this letter, we propose a combined sensing and actuation mechanism for a multi-fingered robotic gripper that borrows the concept of proprioception in the human hand (Fig. 1). The human hand is regarded as a tendon-driven underactuated system that has fewer actuators than the number of degrees of freedom (DOFs) [15], [16], [17], [18], which enables grasping arbitrary objects more efficiently compared to fully-actuated systems, resulting in natural grasping motions. Furthermore, neuroscientists have discovered that the human brain uses predefined synergies instead of controlling each joint of the hand individually due to the complexity of the hand mechanism [19], [20]. We employed two different types of tendons, (non-stretchable) active tendons and (stretchable) passive tendons, in our gripper. Each finger of the gripper is actuated by the active tendon for flexion, whereas the passive tendons perform the task of extending the fingers when the active tendon is released from tension. The active tendon particularly has a function of proprioception directly embedded in the tendon cable, mimicking the GTO of the biological muscle.

The Golgi tendon organ is a proprioceptor of the muscle-tendon unit that detects changes in muscle tension, providing information on the tension of the muscle and autonomously giving feedback to the muscle in real time [21]. In our design,

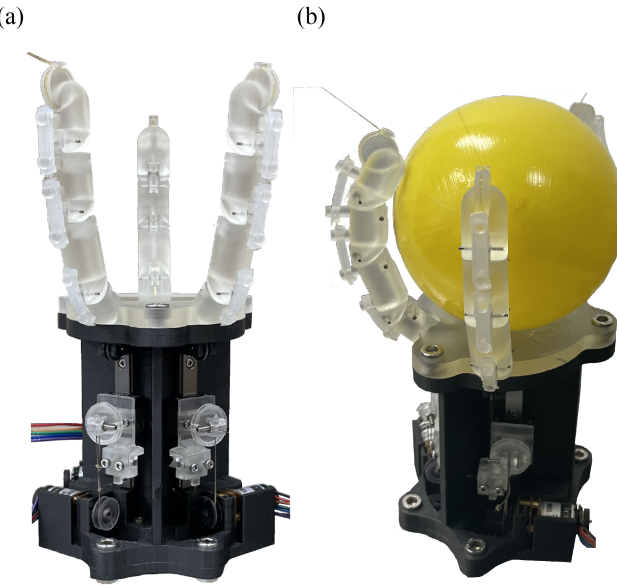


Fig. 1. Prototype of the proprioceptive FBG tendon gripper. (a) Initial state, (b) Grasping a spherical object.

optical fibers with an embedded fiber Bragg grating (FBG) that are highly sensitive to strain changes were employed as the active tendons.

FBGs have been used for force or deflection sensing in robotic devices due to their excellence in strain sensing [22], [23], [24], [25], [26]. FBGs detect strains by measuring the shift of the reflection wavelength of the input light transmitted through optical fibers. Other advantages of FBGs are the structural robustness and the immunity to electromagnetic interference [27], [28], [29]. These characteristics enable the robotic system to retain a lightweight and compact form factor.

Even with these advantages, it is still important to understand the mechanical behavior of the materials of the fiber when using an optical fiber as a tendon of a gripper. Although the optical fiber is flexible, its glass cladding and core are unable to endure a high curvature (i.e., small bend radius); moreover, the polymer coating layer that wraps the core of the fiber may fail if excessive stress is concentrated at a certain point, such as an anchor to the structure. For this reason, the radius of curvature of the optical fiber must not exceed a certain limit, and the stress on the outer coating layer should be well distributed. To accommodate these requirements, we designed a special pulling mechanism with multiple components, including pulleys, round discs, and tendon grooves. While the pulleys and the tendon grooves facilitate smooth curvatures of the tendon, the grooved discs establish stable adhesion of the fiber to the pulling system with increased tensile strength based on Euler's belt formula (i.e., capstan equation) [30], [31], [32].

The goal of this research is to develop a robotic gripper with self-sensing tendons by utilizing the strain-sensitive characteristic of fiber Bragg grating (FBG) sensors. Tendon-driven grippers become bulky and complex when equipped with load cells for fingertip force sensing. However, in our design,

conventional force sensors are replaced with a single strand of a hair-like optical fiber with embedded sensing. Furthermore, the self-sensing active tendon enables the light and compact design of the system by locating the control units away from the device. Therefore, the proposed fiber-optic tendon sensing will be an effective alternative to the complex design and bulky form factor of conventional robotic grippers that require a number of sensors.

## II. DESIGN

The proposed gripper has three fingers, and each finger with three joints has a fiber-optic active tendon on the volar side and three passive elastomer tendons on the dorsal side for extension of the three joints, as shown in Fig. 2(b). The active tendon is pulled by a direct-current (DC) motor, making an underactuated system in each finger.

### A. Finger Design & Tendon Routing

The finger consists of three rigid links, three passive back tendons, and a single active FBG self-sensing tendon. The rigid links were made of transparent methacrylate-based resin (Clear V4, Formlabs) using a 3D printer (Form 3, Formlabs). They were connected with a revolute joint joined by a metal pin (diameter: 1.0 mm) with two ball bearings in each joint as shown in Fig. 2(c). Each joint was designed to have a limit in the range of motion (ROM) between 0° and 45°, avoiding the singularity during the flexion and extension motions.

The finger is actuated by a single active tendon and three passive tendons. The active tendon of the finger, made of an optical fiber, makes finger flexion when pulled by a motor. When the tension on the active tendon is released, the passive tendons with a thickness of 3.0 mm made of soft elastomer (Dragon Skin 10, Smooth-On) pull the links back and make an extension of the finger. The normal distances from the joints to the tendons varied by 2.3 mm, 3.8 mm, and 5.3 mm for the PIP, MCP, and DIP joints, respectively, as shown in Fig. 3(a). These geometric changes resulted in the flexion and extension motions of the three joints in order although the dimensions and the stiffness of the passive tendons are identical.

The optical fiber with an FBG was anchored at the fingertip and located at the volar side of the finger and routed down to the linear guide at the base through multiple filleted holes and several tiny pulleys. A pulley with a diameter of 2 mm was located at each joint of the finger to prevent abrasion of the tendon and to maintain a smooth curvature of the tendon path during flexion since bending of an optical fiber with a small radius might cause critical optical power loss. One end of the fiber-optic tendon was fixed at the fingertip after being wound around a grooved disc. The other end of the fiber was fixed on the linear guide after being wound around another grooved disc. This is to prevent stress concentration on any single point of the fiber, which may result in the delamination of the outer coating from the fiber core. The capstan equation was applied to address this issue. The tension on the fiber when wound around the disc is then

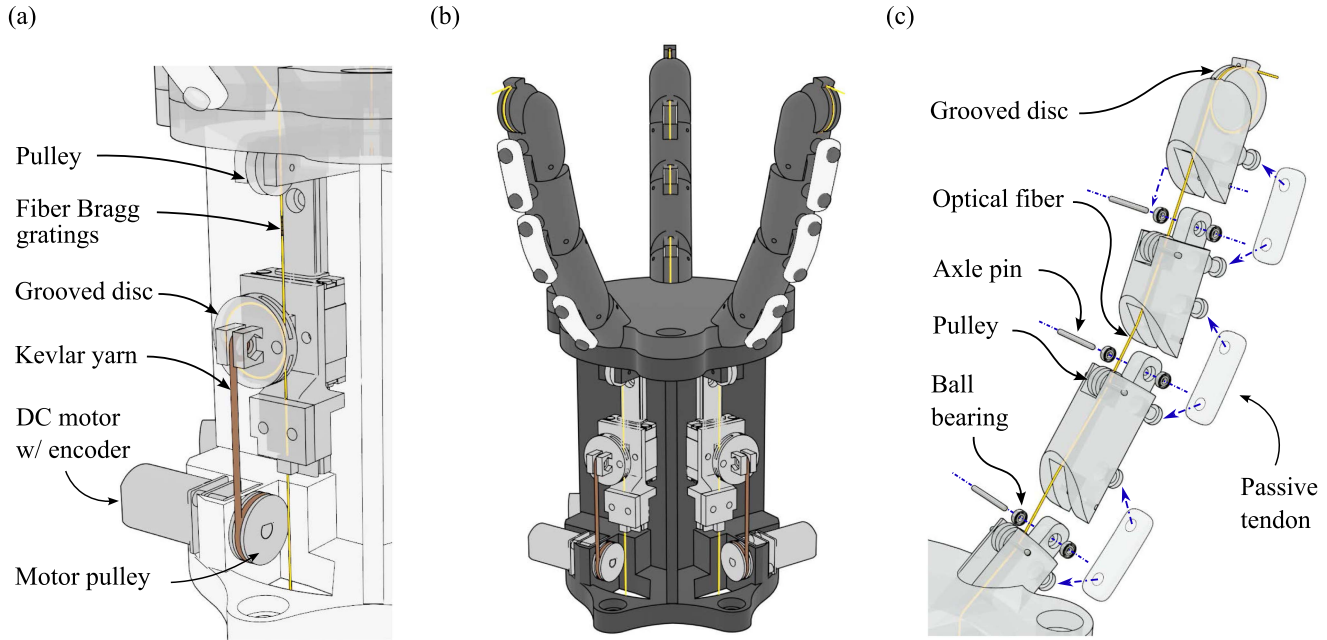


Fig. 2. (a) Important components of the wrist unit. (b) 3D model of the gripper prototype. (c) Exploded view of the finger unit.

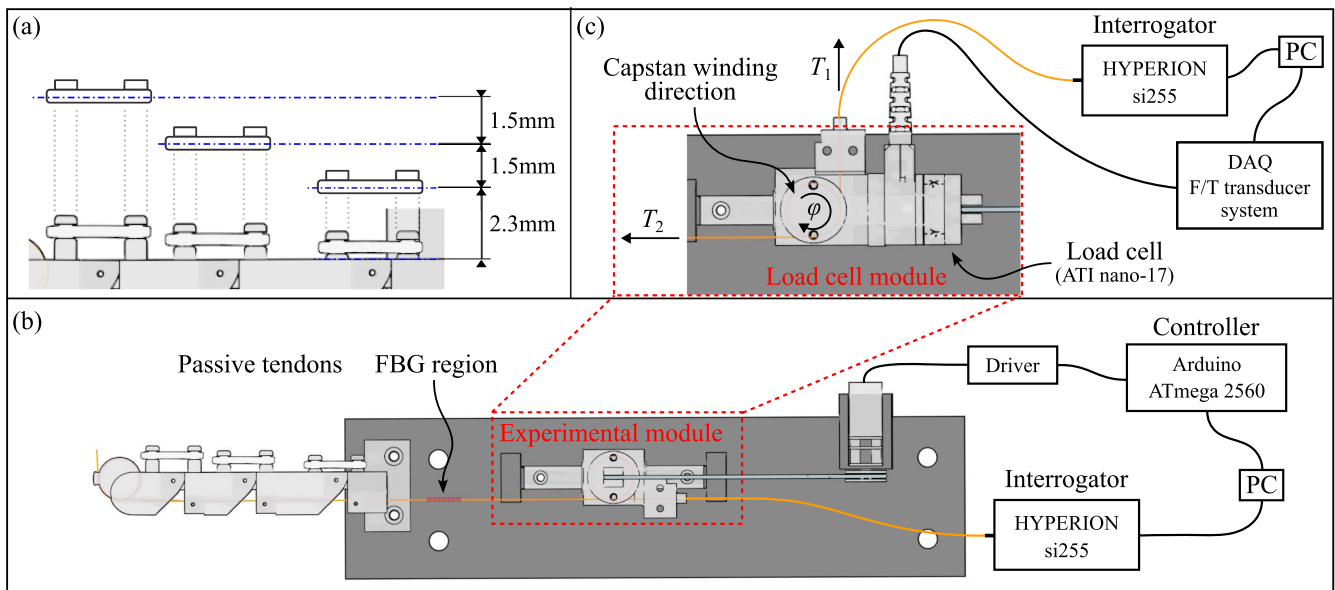


Fig. 3. (a) Dimensions of the passive tendons anchored with different heights for sequential joint actuation. (b) Single finger characterization setup. (c) Load cell module mounted on the linear guide of the testbed for FBG calibration.

expressed as

$$T_2 = T_1 \cdot e^{\mu \cdot \varphi} \quad (1)$$

where  $T_1$  is the resulting force at the other side of the fiber,  $\mu$  is the friction coefficient, and  $\varphi$  is the total angle swept by all turns of the fiber. According to (1), the resulting tension force exponentially increases as the number of windings increases. As a result, the distribution of the clamping force prevented slipping and amputation of the tendon from frictional wear [31]. In addition, the tension of the tendon increases as the diameter of the disc becomes larger, which means the pulling force can be increased for flexion (i.e., enhanced grasping force in actuation).

Selection of the material for the fiber sheath (i.e., fiber coating) and the adhesive was also crucial to the performance of the proposed system [33], [34], [35] to prevent delamination of the coating from the cladding of the fiber, which may result in a failure in force transmission and reduction of the long-term stability of the fiber. Two types of polymer sheaths, acrylate and polyimide, were tested rather than metal sheathing for the flexibility of the tendon. Although the two materials showed a similar performance, polyimide sheath was selected for our tendon, since acrylate did not closely conform to the theoretical model based on the previous research by Weisbitch and Holschemacher [36]. The fiber-optic tendon was attached to each

end point of the grooved disc where the wound fiber ended using fast-hardening two-component epoxy (AXIA EP-04, Alteco). After adhesion, the connector part of the fiber was routed to the FBG interrogator (HYPERION si255, Luna Innovations) for measuring the wavelength shifts of the FBGs.

Kevlar yarn (KEVLAR #3.0, AQUA-X) was tied to the bolt located at the top of the grooved disc on the linear guide in parallel with the tendon. When the motor rotates, the Kevlar yarn pulls the disc mounted on the linear guide and transmits the force to the optical fiber from the DC motor with a shaft diameter of 3.0 mm (RA-12WGM 02TYPE, D&J WITH), connected to a low-cost microcontroller (Arduino Mega 2560, SparkFun Electronics). The target position of the motor shaft was internally controlled using proportional-integral-differential (PID) control with the feedback from the built-in rotary encoder. The encoder value for the initial state was set to zero in the fully extended position of the finger.

### B. Gripper Assembly

Three finger modules, described in Section II-B, were assembled to the base, fabricated with the same material as that of the finger modules, connecting the hand and the wrist of the gripper. The wrist unit, fabricated using a 3D printer (Mark Two, Markforged), consists of pulleys with a diameter of 6.2 mm for the guidance of the path, the linear guide unit including the grooved discs, and the DC motors for actuation, as shown in Fig. 2(a). The guiding pulleys of the wrist part, located below the boundary of the gripper and the wrist, prevent abrasion of the fiber and misalignment of the tendon from the desired path that connects the finger to the linear guide unit. The linear guide unit holds the optical fiber and the Kevlar yarn, wrapped around the motor in the parallel axes.

## III. CHARACTERIZATION

### A. Single Finger Characterization

Fig. 3(b) shows the experimental setup for the characterization of the finger and the FBG sensor. A single finger of the gripper was installed on the testbed comprising only the minimum and essential components to actuate the finger, such as the motor and the linear guide unit. The FBGs were located between the wrist pulley and the linear-guided disc (i.e., set to be untouched) to obtain reliable tension force data of the self-sensing tendon and to prevent damage to the FBG, the most fragile part of the fiber. A high-precision load cell (ATI Nano-17, ATI Industrial Automation) with a resolution of 3.18 mN was tied along the Kevlar line for direct transmission of the force from the motor to the linear guided unit, to calibrate the FBG sensor on the finger.

1) *Tendon Calibration:* The fiber-optic tendon and the Kevlar yarn were aligned in parallel axes to ensure that the FBG sensor data and the load cell data were aligned for calibration, as shown in Fig. 3(c). The fiber-optic tendon was gradually loaded by the motor, and the peak wavelength shifts of the FBG were obtained. The experimental results showed high linearity with the load cell data, showing the  $R^2$  value of 0.997, as shown in Fig. 4(a). The tension data, calibrated from the wavelength

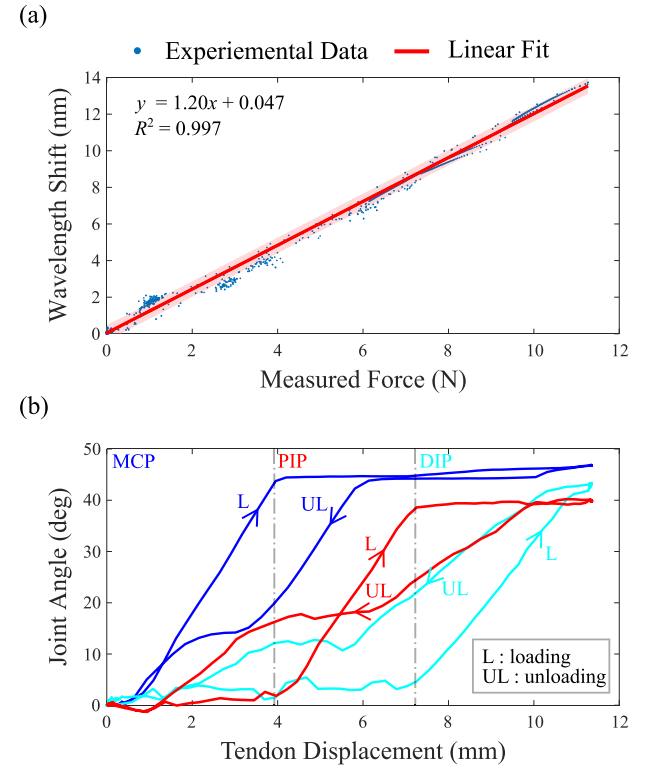


Fig. 4. Single finger characterization. (a) Wavelength shift vs. tension force, measured by the FBG sensor and the load cell, respectively. (b) Sequential finger flexion/extension by each joint.

TABLE I  
MATERIAL PROPERTIES OF TEST SPECIMENS [37], [38], [39]

Material	100% modulus (kPa)
EcoFlex 00-30 (E30)	68.95
EcoFlex 00-50 (E50)	82.74
Dragon Skin 10 (D10)	151.69
Dragon Skin 20 (D20)	268.90
Dragon Skin 30 (D30)	592.95
ONYX	0.64e+6

shifts of the FBG, was exploited for further characterization of the proposed device.

2) *Actuation Performance:* The angles of the MCP, PIP, and DIP joints were estimated using 2D motion analysis software (ProAnalyst, Xcitex). Fig. 4(b) shows the angle changes of the three joints when actuated one by one from MCP to DIP since the normal distance of each passive tendon to the corresponding joint was designed to increase in order. The order of extension is opposite as the tendon is released. Also, the maximum ROM of each joint was restricted up to 45 degrees by the mechanical constraint to prevent the flicking motion of the finger at the singularity caused by the passive tendons during flexion and extension.

3) *Stiffness Sensing:* For testing the performance of stiffness sensing (Fig. 5), six test blocks with different materials for different stiffnesses were prepared, as summarized in Table I.

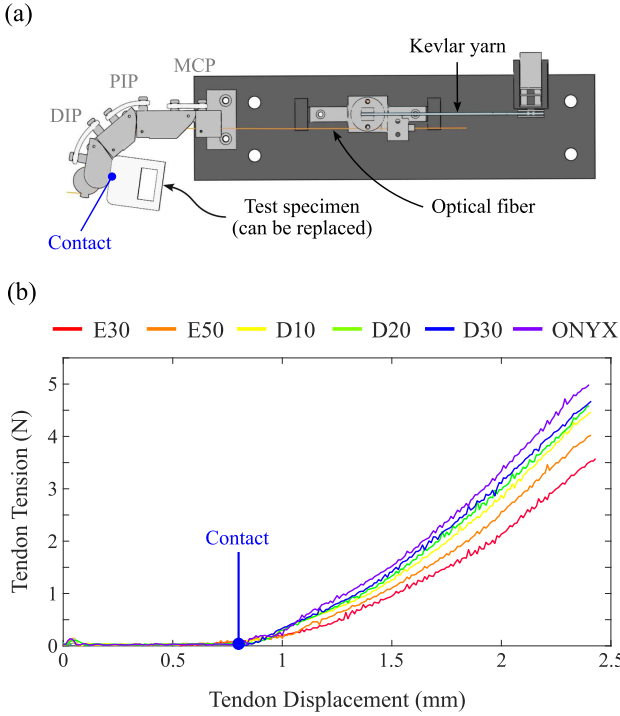


Fig. 5. (a) Stiffness sensing test setup with a single finger and a test block. (b) Tension curves for five test blocks. Each curve shows the mean of 10 trials of finger flexion.

The active tendon was pre-tensioned by bending the DIP and the PIP joints to the maximum angle ( $45^\circ$ ), and a test block was fixed at the fingertip so that further flexion could make the finger apply a normal force to the block, as shown in Fig. 5(a).

The fiber-optic tendon was then pulled by approximately 1.8 mm for 10 times, and the tension on the tendon was measured by the FBG. This test was conducted with all six blocks. Fig. 5(b) shows the mean curve of 10 trials for each block. The finger was able to tell the stiffnesses of the test blocks based on the slopes of the curves, as previously discussed in [40], [41]. The stiffer block showed a steeper slope in the curves. This result demonstrates that the change of the tension measured by the FBG tendon can be utilized to estimate the stiffness of the object to be gripped at the fingertip while it is not easy to directly measure the contact force.

### B. Gripper Characterization

In addition to the single-finger testing, the performance of the three-fingered gripper was evaluated. Balls with different sizes and different stiffnesses were used for grasping, and the tension on one of the fiber-optic tendons was measured while grasping, as shown in Fig. 6(a).

1) *Object Detection*: Balls with two different diameters (73.0 and 83.5 mm) and three different stiffnesses were prepared to evaluate the performance of object detection of the proposed gripper. One of three balls with three different stiffnesses was fabricated of rigid plastic (Onyx, Markforged) by a 3D printer (Mark Two, Markforged), and the other two were made of elastomer (Ecoflex 00-30 and Dragon Skin 10) and by molding

TABLE II  
MATERIAL PROPERTIES OF SPHERICAL OBJECTS [42], [43]

Material	100% modulus (kPa)	Shear Modulus (kPa)	Diameter (mm)
EcoFlex 00-30 (S_E30)	68.95	32.45	73.0
EcoFlex 00-30 (L_E30)			83.5
Dragon Skin 10 (S_D10)	151.69	78.88	73.0
Dragon Skin 10 (L_D10)			83.5
ONYX (S_ONYX)		2.40e+6	73.0
ONYX (L_ONYX)		0.64e+6	83.5

and casting. Table II summarizes the material properties of all six balls. The sensing performance of the gripper was evaluated by the tension measured by the FBG, as shown in Fig. 6(b). When the links of the gripper made contact with an object, the force first increased but stayed similar later due to the slip. Then when the slip ends, the force rapidly increases to make a firm grip.

It was observed that the contact, when the tension first increases, occurred at different displacements depending on the sizes and the materials, as shown in Fig. 6(c). When the tendon of the gripper was pulled by the same displacement (approx. 5.1 mm) for the balls with different sizes, the impact occurred earlier for the large object, resulting in a rapid rise in the slope. The contact point was also different for the materials with the same size due to the high coefficient of friction for soft materials compared to the 3D-printed rigid plastic materials (i.e., less slip on the contact) [44]. Moreover, according to the Dahlquist criterion, soft materials are considered tackier when the shear modulus is below 100 kPa [45]. In other words, less tacky material shows a longer duration of slip. For better comparisons, the experimental data for the materials and the sizes were plotted separately in Fig. 6(d) and (e), respectively. The materials can be distinguished by comparing the slopes and the points where the slope changes.

2) *Control*: Although all the characterization processes were conducted with the position control of the DC motors, the gripper showed a capability of admittance control of the grasping force. The motor velocity was controlled by low-level torque control, a classical proportional-differential (PD) control method. The desired motor velocity,  $\dot{\theta}_{m,des}$ , can be expressed as

$$\dot{\theta}_{m,des} = -K_p e_T - K_d \dot{\theta}_m \quad (2)$$

where  $K_p$  is the proportional gain,  $e_T = T - T_{des}$  is the tension error,  $K_d$  is the differential gain, and  $\dot{\theta}_m$  is the measured motor velocity [46]. The current tension can be acquired from the FBG sensor, while the motor velocity can be obtained from the displacement of the extended tendon over time using the encoder data of the motor, as shown in Fig. 7(a). Fig. 7(b) shows the result of force control that followed the sinusoidal reference signal of frequency 0.5 and 1.0 Hz with a time resolution of 0.04 s respectively. The data on the peak wavelength shifts of the fiber-optic tendons were obtained by the interrogator and transmitted to the main controller, which then sent the information to the microcontroller (Arduino Mega 2560). The

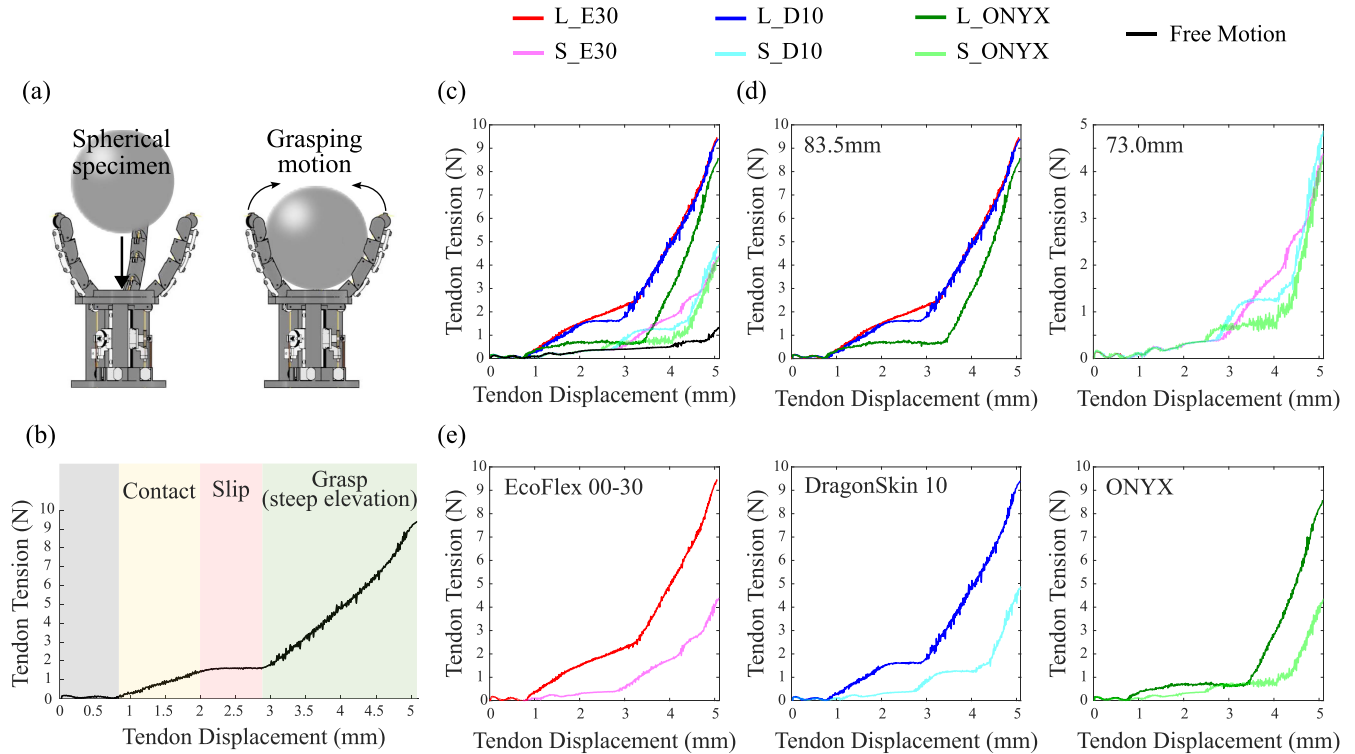


Fig. 6. (a) Experimental setup for grasping test. (b) Tension profiles with the displacement of the tendon while grasping an object (c) Mean curves of tension from 10 cycles per each ball and without any ball (d) Comparisons on the material of the balls of each size (e) Comparisons on the scale of the balls of each material.

microcontroller then used the motor encoder data for feedback control. The processed data were then sent back to the main controller for data recording. Due to the delay in communication between the main controller and the interrogator, the control frequency was found to be 25 Hz, lower than the data sampling frequency of 50 Hz.

The gripper was then integrated with a robotic arm (UR5e, Universal Robots) for testing the control performance during manipulation. In this task, the robot was programmed to sequentially lift an object along the  $z$ -axis and to make translational motions along the  $y$ - and  $x$ -axes in order with a one-second delay after each motion. The robot then returned to its initial position and released the object. The experimental results shown in Fig. 7(c) compare two step-responses without (top) and with (middle) perturbations during control. Despite the disturbances caused by the translational motions in different directions (bottom), the gripper was able to securely hold the object and maintain the desired tension. During the task, the acceleration of the gripper reached up to  $1.8 \text{ m/s}^2$  measured by the inertial measurement unit (IMU) attached to the end-effector of the robot. This shows the performance of force control of the proposed gripper under dynamic conditions.

#### IV. DISCUSSION

The proposed gripper is made of rigid structures with a combination of fiber-optic active and soft passive tendons. The main contribution of our work is demonstrating the feasibility of using an embedded optical fiber as an active tendon of an underactuated tendon-driven gripper, enabling real-time sensing

of tension on the tendon. Optical fibers are strong against tension but fragile when bent sharply. To minimize the structural weaknesses of optical fibers as gripper tendons, various geometric and structural features were taken into our design considerations, especially the location and the curvature of the routes of the optical fiber in the gripper. Moreover, mitigating the damage to the fiber-optic tendon was another important factor in extending the lifespan of the tendons. With the application of Euler's belt formula, the crack and the amputation of the FBG sheath could be prevented by distributing the stress along the fiber wound around the discs and the pulleys. The selection of the adhesive and the material for the sheath of the optical fiber also played an important role in preventing its delamination from the core of the optical fiber. On the other hand, the passive tendons, made of soft elastomer, enabled the sequential flexion of the finger joints which is useful in underactuated systems since this sequence can be easily modulated by changing the locations of the anchors or by using different materials for three passive tendons.

In this research, we discovered several ways of maximizing the durability of the fiber-optic tendon. The diameter of the optical fiber is exceptionally small ( $125 \mu\text{m}$ ) compared to the scale of the proposed device. The fiber-optic tendon, when integrated with the gripper, can be strained up to 15 N. To enhance the grasping force of the gripper, the diameter of the fiber-optic tendon should be tuned to the scale of the gripper or vice versa. Accordingly, if the diameter of the tendon could be customized, the scale of the gripper would not be limited to this extent. Moreover, according to the capstan equation, the durable tension can be significantly improved by increasing the diameter of the round discs or the number of turns.

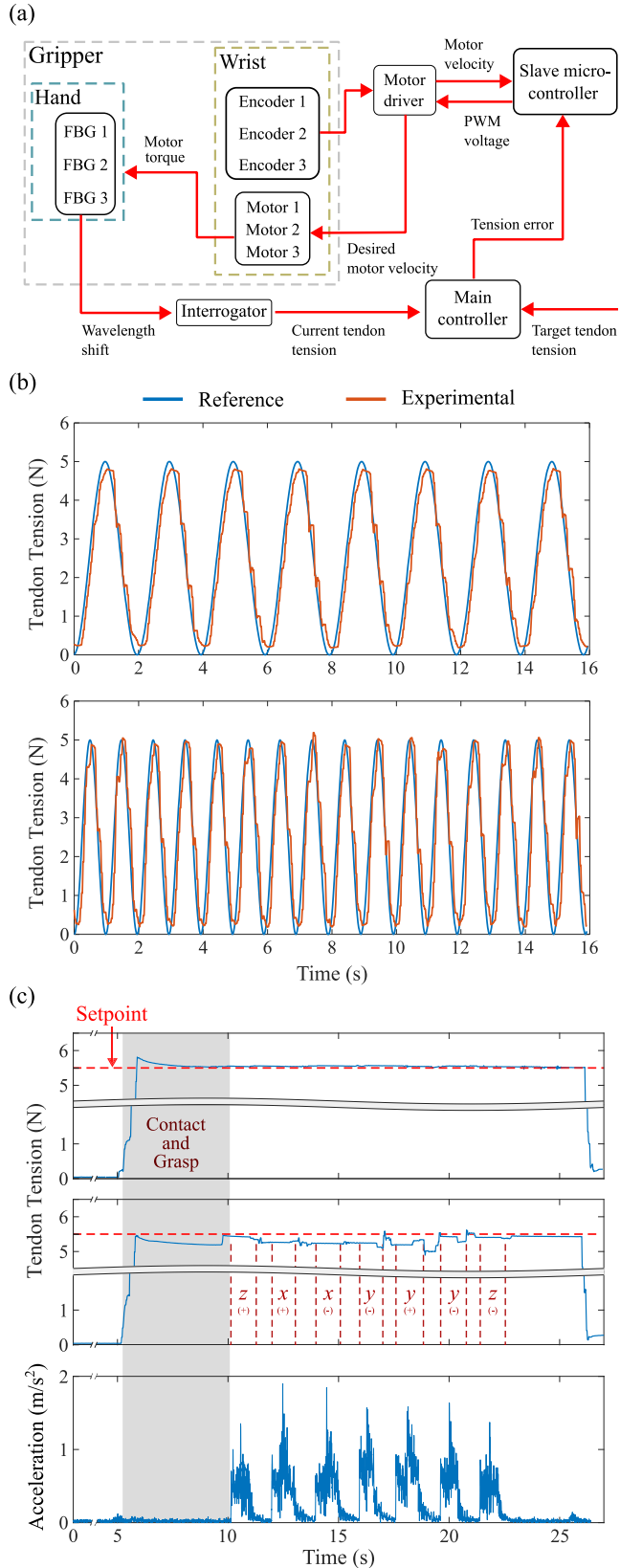


Fig. 7. (a) Block diagram describing the control flow of the gripper system. (b) Comparison of the sinusoidal reference signal of frequency 0.5 Hz (top) and 1.0 Hz (bottom) and the control output. (c) Step responses of the tendon tension during object grasping without (top) and with perturbations (middle). The bottom plot shows the combined ( $x$ ,  $y$ , and  $z$ ) acceleration of the end-effector during the perturbations.

The proposed gripper also showed the capability of distinguishing the stiffnesses of different materials. The slopes of the tension-displacement curves indicated the stiffness values of experimental objects. According to the single-finger result, the slope of the curve increased as the stiffness increased in general. However, as the target material became more rigid, the rate of increase in slope slowed down, indicating a tendency toward saturation.

The gripper experiments showed different shapes in the tension curves as the gripper grasped a ball. As the gripper closed the fingers, the tension first increased but then slowed down due to the slippage between the finger and the ball. Later, the tension rapidly increased until the gripper firmly gripped the ball. These changes in the slopes allowed the detection of different activities of the gripper while grasping.

In this work, we implemented only simple and basic feedback control techniques to evaluate the performance of the proposed device, as low-end motors were used for the prototype. One immediate area of future work will involve building a more dexterous tension-sensing gripper equipped with more powerful motors and constructing an advanced control system. For instance, the delay in communication between the interrogator and the controller, which limited the control frequency, can be mitigated by changing the operating system of the main controller and implementing a high-performance microcontroller. Given that the interrogator can acquire wavelength data at a sampling rate of 1 kHz, the control frequency can be potentially enhanced up to hundreds of hertz in future studies.

To ensure accurate force sensing, active temperature compensation of the FBGs will be a focus of future work as well. In this study, we controlled the ambient temperature to be constant during the experiments. For active temperature compensation, two potential approaches can be considered. The first involves embedding an extra FBG and the use of multiplexing in the same tendon, enabling simultaneous force and temperature sensing. Alternatively, a reference FBG (dual FBG method) can be added to decouple the force-induced strain from the thermal strain [24], [26]. However, when embedding an extra FBG in the same fiber, careful design considerations are necessary to ensure that the thermal sensor remains unaffected by the tension during robot actuation. These active temperature compensation techniques are vital for enhancing both the accuracy and reliability of FBG-based force sensing systems in real-world applications.

Although it is possible to achieve proprioception in the actuation cable using conventional force sensing methods, such as a load cell when the main objective is to gather a single piece of information (e.g., tension). However, the proposed method has a strength in the possibility of expanding the functionality. The fiber-optic tendon with the increased number of FBGs in the future that spans from the wrist to the fingertip will enable the collection of crucial data during grasping and manipulation, including rich tactile information [17], [22] as well as tension data, without increasing the size or adding design complexity to the finger. Another significant advantage of using FBGs for force and tactile sensing is their immunity to electromagnetic interferences (EMI) that enables applications of the proposed gripper in extreme environments [23], [24], [25], [26].

## V. CONCLUSION

We propose a proprioceptive underactuated gripper that includes self-sensing tendons. This research was inspired by the mechanism of Golgi tendon organs in biological muscles. We investigated the efficacy of proprioceptive tendons in an underactuated gripper using FBG sensors. The proposed gripper was able to generate a grasping force of approximately 6 N that was consistent over repeated cycles.

## REFERENCES

- [1] M. R. Cutkosky, *Robotic Grasping and Fine Manipulation*. New York, NY, USA: Springer, 1985.
- [2] A. M. Okamura, N. Smaby, and M. R. Cutkosky, “An overview of dexterous manipulation,” in *Proc. IEEE Int. Conf. Robot. Automat.*, vol. 1, 2000, pp. 255–262.
- [3] O. Khatib and J. Burdick, “Motion and force control of robot manipulators,” in *Proc. IEEE Int. Conf. Robot. Automat.*, 1986, pp. 1381–1386.
- [4] D. Johnston, P. Zhang, J. Hollerbach, and S. Jacobsen, “A full tactile sensing suite for dexterous robot hand and use in contact force control,” in *Proc. IEEE Int. Conf. Robot. Automat.*, 1996, pp. 3222–3227.
- [5] J. S. Son, M. R. Cutkosky, and R. D. Howe, “Comparison of contact sensor localization abilities during manipulation,” *Robot. Autonom. Syst.*, vol. 17, no. 4, pp. 217–233, 1996.
- [6] A. Schmitz, M. Maggiali, L. Natale, B. Bonino, and G. Metta, “A tactile sensor for the fingertips of the humanoid robot iCub,” in *Proc. IEEE/RSJ Int. Conf. Intell. Robots Syst.*, 2010, pp. 2212–2217.
- [7] S. Kröger and B. Watkins, “Muscle spindle function in healthy and diseased muscle,” *Skeletal Muscle*, vol. 11, no. 1, pp. 1–13, 2021.
- [8] E. N. Marieb and K. Hoehn, *Human Anatomy & Physiology*, 8th ed. London, U.K.: Pearson, 2010, pp. 484–490, 514–521.
- [9] M. Park, B. Jeong, and Y.-L. Park, “Hybrid system analysis and control of a soft robotic gripper with embedded proprioceptive sensing for enhanced gripping performance,” *Adv. Intell. Syst.*, vol. 3, no. 3, 2021, Art. no. 2000061.
- [10] J. Jung, M. Park, D. Kim, and Y.-L. Park, “Optically sensorized elastomer air chamber for proprioceptive sensing of soft pneumatic actuators,” *IEEE Robot. Automat. Lett.*, vol. 5, no. 2, pp. 2333–2340, Apr. 2020.
- [11] J. Tapia, E. Knoop, M. Mutný, M. A. Otaduy, and M. Bächer, “Makense: Automated sensor design for proprioceptive soft robots,” *Soft Robot.*, vol. 7, no. 3, pp. 332–345, 2020.
- [12] J. Wirekoh, L. Valle, N. Pol, and Y.-L. Park, “Sensorized, flat, pneumatic artificial muscle embedded with biomimetic microfluidic sensors for proprioceptive feedback,” *Soft Robot.*, vol. 6, no. 6, pp. 768–777, 2019.
- [13] O. Erin, N. Pol, L. Valle, and Y.-L. Park, “Design of a bio-inspired pneumatic artificial muscle with self-contained sensing,” in *Proc. IEEE 38th Annu. Int. Conf. IEEE Eng. Med. Biol. Soc.*, 2016, pp. 2115–2119.
- [14] C. Laschi, “Soft robotics research, challenges, and innovation potential, through showcases,” in *Soft Robotics: Transferring Theory to Applications*, A. Verl, A. Albu-Schäffer, O. Brock, and A. Raatz, Eds. Berlin, Germany: Springer, 2015, pp. 255–264.
- [15] L. Birglen, T. Laliberté, and C. M. Gosselin, *Underactuated Robotic Hands*. Berlin, Germany: Springer, 2007, pp. 1–17.
- [16] S. J. Yoon, M. Choi, B. Jeong, and Y.-L. Park, “Elongatable gripper fingers with integrated stretchable tactile sensors for underactuated grasping and dexterous manipulation,” *IEEE Trans. Robot.*, vol. 38, no. 4, pp. 2179–2193, Aug. 2022.
- [17] L. Jiang, K. Low, J. Costa, R. J. Black, and Y.-L. Park, “Fiber optically sensorized multi-fingered robotic hand,” in *Proc. IEEE/RSJ Int. Conf. Intell. Robots Syst.*, 2015, pp. 1763–1768.
- [18] M. Tavakoli and A. T. de Almeida, “Adaptive under-actuated anthropomorphic hand: ISR-softhand,” in *Proc. IEEE/RSJ Int. Conf. Intell. Robots Syst.*, 2014, pp. 1629–1634.
- [19] M. Santello, M. Flanders, and J. F. Soechting, “Postural hand synergies for tool use,” *J. Neurosci.*, vol. 18, no. 23, pp. 10105–10115, 1998.
- [20] X. Jing, X. Yong, Y. Jiang, G. Li, and H. Yokoi, “Anthropomorphic prosthetic hand with combination of light weight and diversiform motions,” *Appl. Sci.*, vol. 9, no. 20, 2019, Art. no. 4203.
- [21] G. Chalmers, “Strength training: Re-examination of the possible role of golgi tendon organ and muscle spindle reflexes in proprioceptive neuromuscular facilitation muscle stretching,” *Sports Biomech.*, vol. 3, no. 1, pp. 159–183, 2004.
- [22] Y.-L. Park, S. C. Ryu, R. J. Black, K. K. Chau, B. Moslehi, and M. R. Cutkosky, “Exoskeletal force-sensing end-effectors with embedded optical fiber-bragg-grating sensors,” *IEEE Trans. Robot.*, vol. 25, no. 6, pp. 1319–1331, Dec. 2009.
- [23] Y.-L. Park et al., “Real-time estimation of 3-D needle shape and deflection for MRI-guided interventions,” *IEEE/ASME Trans. Mechatron.*, vol. 15, no. 6, pp. 906–915, Dec. 2010.
- [24] E. Aranda-Michel et al., “Miniaturized robotic end-effector with piezoelectric actuation and fiber optic sensing for minimally invasive cardiac procedures,” *IEEE Sensors J.*, vol. 18, no. 12, pp. 4961–4968, Jun. 2018.
- [25] R. Karthikeyan, K. Sigmund, Y.-L. Park, and S. C. Ryu, “Performance evaluation of optically sensorized tendons for articulate surgical instruments,” *J. Med. Devices*, vol. 13, no. 4, 2019.
- [26] J. I. Kim, D. Kim, M. Krebs, Y. S. Park, and Y.-L. Park, “Force sensitive robotic end-effector using embedded fiber optics and deep learning characterization for dexterous remote manipulation,” *IEEE Robot. Automat. Lett.*, vol. 4, no. 4, pp. 3481–3488, Oct. 2019.
- [27] A. D. Kersey et al., “Fiber grating sensors,” *J. Lightw. Technol.*, vol. 15, no. 8, pp. 1442–1463, Aug. 1997.
- [28] K. O. Hill and G. Meltz, “Fiber bragg grating technology fundamentals and overview,” *J. Lightw. Technol.*, vol. 15, no. 8, pp. 1263–1276, Aug. 1997.
- [29] R. Kashyap, *Fiber Bragg Gratings*, 2nd ed. Cambridge, MA, USA: Academic Press, 2009.
- [30] I. M. Stuart, “Capstan equation for strings with rigidity,” *Brit. J. Appl. Phys.*, vol. 12, no. 10, pp. 559–562, 1961.
- [31] A. Horigome and G. Endo, “Basic study for drive mechanism with synthetic fiber rope—investigation of strength reduction by bending and terminal fixation method,” *Adv. Robot.*, vol. 30, no. 3, pp. 206–217, 2016.
- [32] Y.-L. Wang, Y. Tu, and S.-T. Tu, “A study of tensile and fatigue loading effects on the performance of metal-packaged FBG strain sensor developed for cryogenic applications,” *IEEE Sensors J.*, vol. 22, no. 12, pp. 11763–11774, Jun. 2022.
- [33] C. Schilder, M. Schukar, M. Steffen, and K. Krebber, “Structural health monitoring of composite structures by distributed fibre optic sensors,” in *Proc. 5th Int. Symp. NDT Aerosp.*, 2013, pp. 13–15.
- [34] C.-C. Cheng, Y.-L. Lo, B. S. Pun, Y. M. Chang, and W. Y. Li, “An investigation of bonding-layer characteristics of substrate-bonded fiber bragg grating,” *J. Lightw. Technol.*, vol. 23, no. 11, Nov. 2005, Art. no. 3907.
- [35] M. Rasche, *Handbuch Kle 技术*. München, Germany: Carl Hanser Verlag, 2012.
- [36] M. Weisbrich and K. Holschemacher, “Comparison between different fiber coatings and adhesives on steel surfaces for distributed optical strain measurements based on rayleigh backscattering,” *J. Sensors Sensor Syst.*, vol. 7, no. 2, pp. 601–608, 2018.
- [37] Ecoflex™ Series, MSDS, Smooth-On Inc.: Easton, PA, USA, Apr. 14, 2021, Accessed: Nov. 13, 2022. [Online]. Available: [https://www.smooth-on.com/tb/files/ECOFLEX\\_SERIES\\_TB.pdf](https://www.smooth-on.com/tb/files/ECOFLEX_SERIES_TB.pdf)
- [38] Dragon Skin™ Series, MSDS, Smooth-On Inc.: Easton, PA, USA, May. 16, 2022, Accessed: Nov. 13, 2022. [Online]. Available: [https://www.smooth-on.com/tb/files/DRAGON\\_SKIN\\_SERIES\\_TB.pdf](https://www.smooth-on.com/tb/files/DRAGON_SKIN_SERIES_TB.pdf)
- [39] Material Data Sheet: Composites. Watertown, MA, USA: Rev 5.2; Markforged, Jan. 20, 2022. Accessed: Sep. 20, 2023. [Online]. Available: <https://www-objects.markforged.com/craft/materials/CompositesV5.2.pdf>
- [40] L. U. Odhner et al., “A compliant, underactuated hand for robust manipulation,” *Int. J. Robot. Res.*, vol. 33, no. 5, pp. 736–752, 2014.
- [41] M. Vanhees et al., “The effect of displacement on the mechanical properties of human cadaver subsynovial connective tissue,” *J. Orthop. Res.*, vol. 30, no. 11, pp. 1732–1737, 2012.
- [42] R. R. Fernandes, A. Y. Tamjani, and M. Al-Haik, “Mechanical characterization of additively manufactured fiber-reinforced composites,” *Aerospace Sci. Technol.*, vol. 113, 2021, Art. no. 106653.
- [43] L. Marechal, P. Balland, L. Lindenroth, F. Petrou, C. Kontovounios, and F. Bello, “Toward a common framework and database of materials for soft robotics,” *Soft Robot.*, vol. 8, no. 3, pp. 284–297, 2021.
- [44] Q. Lu, A. B. Clark, M. Shen, and N. Rojas, “An origami-inspired variable friction surface for increasing the dexterity of robotic grippers,” *IEEE Robot. Automat. Lett.*, vol. 5, no. 2, pp. 2538–2545, Apr. 2020.
- [45] C. W. Paul, “Pressure-sensitive adhesives (PSAs),” in *Handbook of Adhesion Technology*, L. F.M. da Silva, A. Öchsner, and R. D. Adams, Eds. Berlin, Germany: Springer, 2011, pp. 341–372.
- [46] J. Zhang, C. C. Cheah, and S. H. Collins, “Experimental comparison of torque control methods on an ankle exoskeleton during human walking,” in *Proc. IEEE Int. Conf. Robot. Automat.*, 2015, pp. 5584–5589.